Effect of shear flow on the hydrodynamic drag force of a spherical particle near wall evaluated using optical tweezers and microfluidics

Lester C. Geonzon, Motoyoshi Kobayashi *, Yasuhisa Adachi

School of Life and Environmental Sciences, University of Tsukuba

1-1-1 Tennodai, Tsukuba, Ibaraki, 305-8572, Japan

*Corresponding author:

Name: Motoyoshi Kobayashi, Ph.D.

E-mail Address: kobayashi.moto.fp@u.tsukuba.ac.jp

Tel & Fax: +81-(0)29-853-5721

Address: Faculty of Life and Environmental Sciences, University of Tsukuba

1-1-1 Tennodai, Tsukuba, Ibaraki, 305-8572, Japan

Abstract

The hydrodynamic drag force on a spherical particle in shear flow near-wall is investigated using optical tweezers and microfluidics. Simple shear flow is applied using a microfluidic channel at different volumetric flow rates. The hydrodynamic drag force exerted on the particle is detected from the displacement of the trapped particle. The effect of the wall is obtained from the force balance of the trapping and hydrodynamic drag force employing the exact solution of the theoretical model using the lubrication theory for a sphere near the wall. Here, we report the experimentally obtained hydrodynamic drag force coefficient under the influence of shear flow. The drag correction factor increases with decreasing distance from the wall due to the effect of the wall surface. We found that the calculated hydrodynamic drag force coefficient is in quantitative comparison with the theoretical prediction for a shear flow past a sphere near-wall. This study provides a straightforward investigation of the effect of the shear flow on the hydrodynamic drag force coefficient on a particle near the wall. Furthermore, these pieces of information can be used in various applications, particularly in optimizing microfluidic designs for mixing and separations of particles or exploit the formation of the concentration gradient of particles perpendicular to flow directions caused by the non-linear hydrodynamic interactions

Keyword: Hydrodynamic shear flow/Optical tweezers/microfluidics/drag force

1. Introduction

Flow of colloidal suspension is a fundamentally and practically essential process that is present in a plethora of applications. The flow of colloidal particles in rivers,[1,2] transport of particles in filtration,[3] microfluidic flows in biomedical devices,[4,5] and the flow of blood cells in the body, to name a few, are the important natural and technological settings of the flow of colloids. Common to all these applications, adhesion or deposition[6-10] of colloidal particles onto the surface in contact with the flow is one of the most critical issues—for example, adhesion of cells to tissues in bloodstreams is essential to many pathophysiological processes,[11,12] or the "tubular pinch" effect of diffusing spherical particle in Poiseuille flow along a narrow gap annulus is vital in membrane technology.[13,14] Even though the kinetics of deposition of colloidal particles is influenced by several factors like flow conditions, surface chemistry, and particle volume fraction, it is widely recognized that particle-wall interactions generally define the system. Hence, understanding the effect of hydrodynamic forces on a particle in the vicinity of a wall translating by a shear flow is of fundamental importance.

Accordingly, several numerical models based on fluid dynamics have been proposed to estimate the forces and torques on particles translating near-wall. Dean and O'Neill[15] addressed the issue of the flow around a rotating sphere near-wall using bipolar coordinates. Moreover, O'Neill[16] explicitly determined the hydrodynamic forces about the fixed sphere in contact with fluid motion using the exact solution of the linearized Stokes flow equations. These issues are revisited by Goldman *et al.*,[17,18] incorporating the lubrication theory for an extended analysis in the case wherein the gap between the particle and wall is smaller than the particle radius in a quiescent and Couette flow. O'Neill and Stewartson[19,20] further reconsidered the lubrication problem by matched asymptotic expansions and Perkins and Jones[21] using the terms of the Green function for bounded fluid. Additionally, Magnaudet *et al.*[22] evaluated the slip and shear effects in wall-bounded flows to infer the hydrodynamic drag on a fixed particle. Later, Chaoui and Feuillebois[23] re-examined the creeping flow around a sphere using bipolar coordinates with improved numerical calculations, wherein the earlier results were recovered with a precision order of 10^{-11}.

On one side, a large number of numerical simulations have been performed to verify the hydrodynamic drag force on the flowing particle near-wall.[24-30] Zeng *et al.*[25] performed direct numerical investigations on the hydrodynamic drag force on a particle in a linear shear flow with finite slip at near wall. Recently, Ekanayake *et al.*[30] numerically evaluated the drag and lift forces on a particle near the wall in shear flow with an improved wall-shear-based drag correlation. The method accurately captures the drag force and follows the results of the theoretical models. However, experimental studies evaluating the hydrodynamic drag force on the particle under the influence of shear flow are relatively scarce due to the difficulty in determining the actual forces in situ. Although some methods are utilized to understand the hydrodynamic drag force of the particle near-wall, such as studies on hydrodynamic interactions in quiescent or uniform flow conditions,[31-33, 49-50] to the best of our knowledge, no detailed investigations are performed to evaluate the hydrodynamic drag force exerted on a particle near a wall under shear flow. Hence the motivation of this study is a direct evaluation of the hydrodynamic force on a particle near a wall under shear flow, which is very important in a plethora of applications.

Optical tweezers have become an essential tool in various fields due to their versatile applications.[34-40] With the advent of optical trapping and microfluidics, diverse applications ranging from chemistry and physics to medicine and biology have become available. One of the most emerging lab-on-a-chip device applications controls and manipulates colloidal particles under varying flow fields and solution environments. From this standpoint, a micrometer-sized particle can be trapped, and the displacement of the particle in the trap is a measure of the force exerted on it. Hence the corresponding forces felt by the trapped particle can be exploited to characterize the surrounding environment.[39,40] Additionally, with the increasing applications of microfluidic devices, it is important to evaluate the effect of these hydrodynamic interactions between particle and wall. Precise control over particle position in microfluidic devices allows for more efficient and high throughput operations on flowing objects in microchannels. Therefore, with optical trapping and precise control of fluid flow using microfluidics, it is ideally possible to directly evaluate the hydrodynamic drag force exerted on a particle under shear flow at any location within the channel.

Therefore, this study aimed to investigate the hydrodynamic drag force on a colloidal particle within the vicinity of a near-wall under the influence of shear flow using optical tweezers and microfluidics. Even though this is a classical problem, to the best of our knowledge, a quantitative comparison between theoretical and experimental measurements has not been reported to date. A significant advantage of this study stems from its ability to directly measure the total force acting on the particle under shear flow. Furthermore, back-focal-plane detection in optical tweezers provides high temporal and spatial resolution for the force measurements. Hence, we report on the experimentally obtained drag correction factor and compare it with the theoretical model and numerical calculations on the particle-wall interaction under shear flow to further extend the previous measurements of the translational drag coefficient.

2. Materials and Methods

2.1 Experimental setup

An optical trapping kit (OTKB/M, Thorlabs) equipped with a single laser (wavelength λ=976 nm) was used in the experiments. The laser light was delivered to the system via an SM980-5.8-125 single-mode fiber (Thorlabs). A 100× oil immersion objective with a high numerical aperture (NA 1.25, WD 0.23 mm, Nikon) was used to tightly focus the laser beam. An air condenser (10×, NA

0.25, WD 7 mm, Nikon) was used to collect the laser light passing through the sample and further reflected into the quadrant position detector (QPD) using a dichroic mirror for the back-focal plane detection (OTKBFM, Thorlabs). The QPD was connected to the force measurement module (OTKBFM-CAL, Thorlabs) for data acquisition. The time-series signals of the x- and y-displacement of the particle in the trap were recorded at a rate of 10 kHz for at least ten seconds using the software package for the OTKBFM-CAL Force Acquisition Module (OTKB-Cal, Thorlabs). A piezo-controlled 3-dimension translational stage (NanoMax 300, Thorlabs) was used to position the micro-channel with respect to the optical trap using the Thorlabs APT software package. The particle position was controlled using the piezo-controlled 3-dimensional stage in stepwise increments with a readout resolution of 0.32±0.02 μm/V. The axial distance of the particle relative to the surface of the channel bottom, h/a, where h is the axial distance of the centroid of the particle from the bottom surface of the inner wall, and a is the particle radius, was calibrated manually by moving the stage. In this way, the axial distance h was controlled while the position of the particle was kept constant using the optical trap.

The voltage fluctuation of the trapped particle was converted into particle displacement using the QPD calibration factor. The voltage-to-position response function of the QPD was calibrated by displacing the particle at the equilibrium position in the trap using fluid flow. The constant particle displacement was measured by image processing, and the QPD signal was recorded. The slope of particle displacement (μm) as a function of QPD response (V) was determined to be 0.48 V/μm (see Supplementary Fig. 1).

The probe particles used in the experiments were non-functionalized silica (diameter $2a$=2.5 μm, Nippon Shokubai, Japan) suspended in pure water. Silica particles are negatively charged in aquatic solution [41,42,] and the double layer repulsion reduces the adhesion of silica to a glass surface. Particle suspensions were prepared by diluting the stock suspension of 0.1 wt.% to 0.0001 wt.%. Deionized water (Elix Advantage 5, Millipore, Tokyo, Japan) was used to prepare all particle suspensions. All the experiments were conducted at room temperature (20 °C).

2.2 Flow measurements

Flow experiments were performed using a parallel flow chamber (sticky-Slide I, 0.1 Luer, Part of: 81128, Ibidi, Germany) with channel dimensions (length L=48000 μm, width W=5000 μm, and total height H=150 μm, including the double sticking tape). The glass coverslip (#1, 0.12~0.17 mm, NEO, Matsunami, Japan) was attached to the flow cells by double sticking tape (thickness =50 μm). Coverslips were used as provided by the manufacturer without any surface modifications. The flow chamber and coverslip were tightly compressed and incubated at 40 °C overnight to obtain strong adhesion, following the recommendation of the manufacturer (Ibidi, Germany). The microchannel was connected to a 1 mL plastic syringe (inner diameter =4.65 mm, Soft-ject, Henke-Sass Wolf, Germany) using silicone tubing. Particle suspensions were injected into the flow cell using a high-precision syringe pump (Nexus 3000, Chemyx Inc., USA). A random particle was trapped at a fixed laser current of 250 mA. After that, pure water was flowed into the channel to flush the remaining particles to remove interparticle interaction during the measurements. The flow measurements were performed at different volumetric flow rates at 500 μL/hr, 1000 μL/hr, and 1500 μL/hr, respectively. The displacement of the particle at various *h/a* with respect to the equilibrium position was recorded for at least ten seconds.

2.3 Stiffness calibration

The position at which the particle touched the surface (*h/a* = 1) was determined from the drastic change in the QPD signal.[30,41]After determining the reference position, *h/a* = 1, the particle position was then changed to *h/a* ~ 10 by moving the stage. After that, the particle fluctuation was recorded for at least ten seconds, and the corresponding trap stiffness was determined using the power spectral density (PSD) roll-off method.

The optical trap stiffness was calibrated at various *h/a*, as shown in Fig. 1. The laser current was set to 250 mA for the trapping. The measured trap stiffness *k* showed a weakening with increasing *h/a*. This dependence is expected for an oil-immersion objective due to spherical aberrations caused by the refractive index mismatch, which agrees with the previous results.[37,43] Therefore, the fitting line in Fig. 1 is used to obtain the actual trap stiffness *k*(*h/a*).

3. Results and Discussion

3.1 Hydrodynamic effect near-wall at the quiescent condition

The hydrodynamic effect on the particle near the wall is investigated by following the change in the thermal fluctuation of the trapped particle as it is brought closer to the wall. Fig. 2a presents the representative 1-dimensional time-series fluctuation of an optically trapped particle without shear flow at representative *h/a*. An apparent attenuation in the thermal fluctuation could be observed as the particle approaches the wall due to the hydrodynamic effect.

The thermal fluctuation of the trapped particle is analyzed to quantify the change in the hydrodynamic drag using the normalized position autocorrelation function (NPAF),[40, 51] described as follows:

$$A(\tau) = \frac{\langle \vec{x}(t)\vec{x}(t+\tau)\rangle_t}{\langle x^2\rangle_t} \quad (1)$$

where $\vec{x}(t)$ is the particle position at time *t*, τ is the time interval (lag-time) a nd $\langle x^2\rangle$ is the time-independent variance of the particle. Based on the assumption of a sufficiently long measurement (i.e., larger than 1/λ) of the thermal fluctuation of the particle in a Newtonian fluid with constant viscosity, the NPAF can be approximated by a single exponential decay[40, 51]

$$A(\tau) = e^{-\lambda\tau} \quad (2)$$

where $\lambda = k/\gamma$, *k* is the trap stiffness, and $\gamma=6\pi a\eta$ is the drag coefficient where η is the fluid viscosity. Correspondingly, the characteristic λ is directly related to the relaxation rate of the system, also known as the *corner frequency,* when the particle fluctuation is analyzed in terms of the power spectral density.[40,44,46]

The normalized γ/γ_0 as a function of *h*/*a* is shown in Fig. 2b. The measured drag coefficient γ is normalized using the value of γ farthest from the surface, γ_0. The data for λ_0/λ is also shown for reference. Since the k varies with h/a, the corresponding γ is calculated using the actual $k(h/a)$ obtained in the calibration. As Fig. 2b shows, the γ/γ_0 increases dramatically at a distance close to the wall because of the hydrodynamic friction, and at the same time, it is constant at approximately large distances. The normalized γ/γ_0 is compared with the theory for a particle moving parallel to the wall by Goldman *et al.*[17] and Faxen's correction for lateral directions. The results are in good agreement and consistent with the expectations from the hydrodynamic theory. Hence, the attenuation of the thermal fluctuation of the trapped particle as it is brought closer to the wall is due to the hydrodynamic interactions between the particle and the surface. Accordingly, these results were consistent with the previous studies,[35,47,49-50] confirming the applicability of our methodology to investigate the hydrodynamic interactions between the particle within the vicinity of a wall in a more complicated scenario such as under shear flow conditions.

3.2 Hydrodynamic effect near-wall by shear flow

The more complex hydrodynamic interactions between a spherical particle and wall under simple shear flow are evaluated. Simple shear flow is obtained from the gradient of the fluid velocity close to the wall. Considering no-slip boundary conditions, the fluid velocity profile in a rectangular channel is accessible as an analytical solution of the Navier-Stokes equation for a pressure-driven flow. The fluid velocity in the x-direction can be expressed as follows:[48, 52]

$$U_x(y,h) = \frac{4H^2\Delta p}{\pi^3\eta L}\sum_{n,odd}^{\infty}\frac{1}{n^3}\left[1-\frac{\cosh\left(n\pi\frac{y}{H}\right)}{\cosh\left(n\pi\frac{W}{2H}\right)}\right]\sin\left(n\pi\frac{yh}{H}\right) \qquad (3)$$

with H, W, L, and η as previously defined, and $\Delta p/L$ is the pressure gradient. The pressure gradient $\Delta p/L$ is further defined in terms of the volumetric flow rate, Q, given as follows: [48, 52]

$$Q = \frac{H^3 W \Delta p}{12\eta L}\left[1 - \sum_{n,odd}^{\infty}\frac{1}{n^5}\frac{192}{\pi^5}\frac{H}{W}\tanh(n\pi\frac{W}{2H})\right]. \tag{4}$$

The theoretical fluid velocity within the channel is plotted in Fig. 3. At distances close to the channel walls, the fluid velocity increases almost linearly; thereby, it is defined as a simple shear flow. The calculated fluid velocity at different *h/a* was also confirmed experimentally at a volumetric flow rate of 500 μL/hr by tracking the flowing particle after being released in the trap, as shown in the open symbol in Fig. 3. A good agreement between the predicted and experimentally obtained local fluid velocity is shown. Additionally, due to the relatively thick microfluidic channel in comparison to the working distance of the optical trap, the measurement was performed at the limited axial range of *h/a*. Nevertheless, the fluid velocity linearly increases within the observation range of *h/a*; therefore, this method can be utilized to apply a simple shear flow on a particle within the vicinity of the wall.

Fig. 4 presents the displacement of the trapped particle, Δx, from its equilibrium position at various *h/a* for different volumetric flow rates Q. In general, when an external force is applied to the trapped particle, the particle displacement from the equilibrium point is proportional to the applied force. Also, it has been shown that the optical trap can be treated approximately as a linear spring where the force F_{trap}, is given by $F_{trap} = k\Delta x$ where k is previously defined.

In Fig. 4, the Δx increased with increasing *h*/*a* for all volumetric flow rates. This increase corresponds to the applied hydrodynamic force by shear flow. Based on the linearity of Stokes' equation, the external force acting on the trapped particle is due to the hydrodynamic resistance force (drag force). For an unbounded fluid flow or at large *h/a*, the drag force is only a function of fluid velocity. However, for a particle translating near the wall, the drag force exerted on the particle is affected by the presence of the boundary surfaces, which nonlinearly modifies the hydrodynamic drag exerted by the fluid.

The analytical solution of the hydrodynamic drag force exerted on a particle near wall in a simple shear flow is expressed as follows:[18]

$$F_d = 6\pi a\eta U_x f^*(h/a) \tag{5}$$

where a and η is previously defined, U_x is the fluid velocity and $f^*(h/a)$ is the correction factor of the drag friction coefficient, which is a function of *h/a*. The $f^*(h/a)$ in Eq. 5 is considered highest when the particle is in contact with the wall and decays rapidly to the unbounded value as the *h/a* increases.[18] Using the exact value of U_x at *h/a*, the $f^*(h/a)$ was calculated by taking the force balance between the trapping force and the effective drag force wherein the total force acting on the particle is given as follows:

$$k\Delta x = 6\pi a\eta U_x f^*(h/a). \tag{6}$$

Fig. 5 presents the f^* as a function of *h/a* between the particle and the wall. Also plotted for comparison in the Figure as a solid line is the exact solution of the theoretical model obtained by Goldman *et al.*[18] From Fig. 5, it is clear that the drag force increases with decreasing *h/a* between the particle and the wall. When the particle is near the vicinity of the wall, the space between the particle and the surrounding fluid is reduced; hence, increasing the corresponding drag force in a direction parallel to the wall. Therefore, the total drag force experienced by the particle is observed to be increased by the presence of the wall, while beyond that, the particle experiences an unbounded fluid flow. The experimentally calculated f^* over the range of h/a is in good agreement with the theoretical values of Goldman *et al.*,[18] verifying the applicability of the theoretical model.

Furthermore, the hydrodynamic drag force coefficient did not show any dependency for the studied volumetric flow rates. Based on the force balance equation between the trapping and drag force in Eq. 6, the force felt by the particle is only a function of the fluid velocity at a certain distance, which is proportional to the displacement in the optical trapping force. Thereby, the volumetric flow rate increase would only mean an increase in the applied drag force at laminar flow conditions and, consequently, the displacement Δx as shown in Fig. 3. This reflects the independence of the calculated hydrodynamic drag coefficient on the volumetric flow rate, at least at laminar flow conditions. Moreover, this independence also corroborates the assumption of the theoretical model wherein no-slippage, Newtonian fluid flow, and low Reynold's number conditions are satisfied. However, for conditions where slippage, non-Newtonian fluid, or large Reynold's number cases is considered, this independence might be affected.[53]

Although it is well known that shear flow on a particle near the wall can also induce torque and lift force,[18, 25,30] such effects are not considered in the present analysis. For a spherical particle made of homogenous, transparent isotropic material, optical torque is not considered; thus, the particle rotation and torque are not considered in the present analysis. Meanwhile, the lift force is assumed nullified by the optical trapping force, limiting the axial displacement of the particle while under the influence of shear flow. Thus, here we only ponder that the drag force influences the particle dynamics predominantly. Moreover, Goldman *et al*.[18] independently considered the effect of hydrodynamic drag and toque. Therefore, Eq. 5 is derived solely for the hydrodynamic drag force exerted by the fluid on the particle. However, the effect of torque and lift force is similarly important and should be considered in future research, especially in non-steady flow conditions and in non-Newtonian fluids.[53]

It is also important to compare our results with the earlier study of Eom *et al*.[45] using optical tweezers to probe the fluid flow. However, the experimental range of their study was a lot larger than the present study; thus, the effect of near-wall was not accounted for in their analysis. Nevertheless, the technique using optical tweezers and microfluidics provides the direct force measurement on the hydrodynamic drag force exerted on a particle near-wall under shear flow. From an applied perspective, understanding the hydrodynamic interactions in different flow conditions is very important, particularly in microfluidics applications, where colloids are used for various applications. Since most studies focus on the hydrodynamic interactions in quiescent conditions or homogeneous flow, in this study, we report on the effect of the shear flow condition, a kind of simplest inhomogeneous flow field, on the hydrodynamic drag force, on the particle within the vicinity of the wall. These pieces of information can be utilized to optimized microfluidic designs for mixing and separations of particles or exploit the formation of the concentration gradient of particles perpendicular to flow directions caused by the non-linear hydrodynamic interactions. Finally, the present results may be utilized as an alternative method for force calibration for the optical trap.

4. Conclusion

Combining optical trapping equipped with force detection and a microfluidic channel is utilized to quantitatively evaluate the hydrodynamic drag force on a particle near the wall in a quiescent and shear flow environment. The calculated drag friction coefficient increases with decreasing distance from the wall due to the increased hydrodynamic effect. For particle-wall interaction without shear flow, the change in the drag coefficient is well represented by the theoretical prediction and coincides with the previous studies. In the case of particle-wall interaction under shear flow, the experimentally calculated drag friction coefficient is in quantitative agreement with the exact solution of the theoretical model of Goldman *et al.* (1967b). These findings provide a straightforward force measurement technique for verifying the hydrodynamic drag force coefficient, which is further available to calibrate optical trapping force under shear. Furthermore, with the advent of lab-on-a-chip devices, this result will provide helpful information in quantifying the effect of the wall and controlling the particle in the microfluidic flow. This can be used to optimized microfluidic designs for mixing and separations of particles or exploit the formation of the concentration gradient of particles perpendicular to flow directions caused by the non-linear hydrodynamic interactions for high throughput operations.

Author Contributions

Lester C. Geonzon: Conceptualization; Data curation; Formal analysis; Methodology; Software; Validation; Visualization; Writing-original draft; Writing-review & editing. **Motoyoshi Kobayashi**: Supervision; Conceptualization; Formal analysis; Visualization; Writing-original draft; Writing-review & editing; Resources; Funding acquisition; Project administration. **Yasuhisa Adachi**: Supervision, Resources; Funding acquisition; Project administration.

Conflicts of interest

There are no conflicts to declare.

Acknowledgment

The authors are grateful for the financial support of JSPS KAKENHI Grant Number 20F20388 and 19H03070.

References

1. R. Beckett, G. Nicholson, B. T. Hart, M. Hansen and J. C. Giddings, *Water Research*, 1988, **22**, 1535-1545.
2. G. Karaiskakis, K. A. Graff, K. D. Caldwell and J. C. Giddings, *International Journal of Environmental Analytical Chemistry*, 1982, 12, 1-15.
3. H. M. Wyss, D. J. Blair, J. F. Morris, H. A. Stone and D. W. Weitz, *Phys. Rev. E*, 2006, 74, 061402.
4. A. A. S. Bhagat, H. W. Hou, L. D. Li, C. T. Lim and J. Han, *Lab Chip*, 2011, **11**, 1870-1878.

5. S. N. Bhatia and D. E. Ingber, *Nature Biotechnology*, 2014, **32**, 760-772.
6. K. E. Nelson and T.R. Ginn, *Langmuir*, 2005, 21, 2173-2184.
7. Z. A. Kuznar, and M. Elimelech, *Colloids and Surf. A*, 2007, **294**, 156-162.
8. M. Kobayashi, H. Nanaumi and Y. Muto, *Colloids and Surf. A*, 2009, **347**, 2-7.
9. L. C. Geonzon, R. G. Bacabac and S. Matsukawa, *Journal of Electrochemical Society*, 2019, **166**, B3228.
10. L. C. Geonzon, A. Santoya, X. Zhuang, J. Xie, R. G. Bacabac and S. Matsukawa, *Food Hydrocolloids*, 2020, **105**, 105759.
11. S. Huang and D. E. Ingber, *Nat Cell Biol*. 1999, **1**:E131-8.
12. A. A. Khalili and M. R. Ahmad, *Int J Mol Sci*, 2015, **16**, 18149-18184.
13. Y. S. Choi and S. J. Lee, *Microfluid Nanofluid*, 2010, **9**, 819-829.
14. L. Clime, K. J. Morton, X. D. Hoa and T. Veres, *Scientific Reports*, 2015, **5,** 9765.
15. W. R. Dean and M.E. O'Neill, *Mathematika*, 1963, **10**, 13.
16. M. E. O'Neill, *Mathematika*, 1964, **11**, 67.
17. A.J. Goldman, R. G. Cox and H. Brenner, *Chem. Eng. Sci*., 1967a, **22**, 637-651.
18. A.J. Goldman, R. G. Cox and H. Brenner, *Chem. Eng. Sci*., 1967b, **22**, 653-660.
19. M. E. O'Neill and K. Stewartson, *J. Fluid Mech*., 1967, **27**, 705-724.
20. M. E. O'Neill, *Chem. Eng. Sci.*, 1968, **23**, 1293-1298.
21. G. S. Perkins and R. B. Jones, *Physica A*, 1992, **189,** 447-477.
22. J. Magnaudet, S. H. U. Takagi and D. Legendre, *J. Fluid Mech*., 2003, **476,** 115-154.
23. M. Chaoui and F. Feuillebois, *Q. J Mech. App. Math*, 2003, **56**, 381-410.
24. R. Kurose and S. Komori, *J. Fluid Mech.*, 1999, **384**, 183-206. DOI:
25. L. Zeng, F. Najjar, S. Balachandar and P. Fischer, *Phys. Fluid*, 2009, **21**, 033302.
26. F. Takemura and J. Magnaudet, *Phys. Fluid*, 2009, **21**, 083303.
27. H. Lee and S. Balachandar, *J. Fluid Mech.,* 2010, **657**, 89-125.
28. O.B. Bocharov and D.Y. Kushnir, *Thermophysics and Aeromechanics*, 2016, **23**, 83-95.

29. Z. Zhou, G. Jin, B. Tian and J. Ren, *Int. Journal of Multiphase Flow*, 2017, **92**, 1-19.
30. N. I. K. Ekanayake, J. D. Berry, A. D. Stickland, D. E. Dunstan, I. L. Muir, S. K. Dower and D. J. E. Harvie, *J. Fluid Mech.,* 2020, **904**, A6.
31. P. Huang, J. Guasto and K Breuer, *J. Fluid Mech.,* 2006, **566**, 447, 464.
32. P. Huang and K. Breuer, *Phys. Rev. E,* 2007, **76**, 043607.
33. S. Adarwa, H. B. Tabrizi and G. Ahmadi, *Particuology*, 2014, **16**, 84-90.
34. A. Ashkin and J. M. Dziedzic, *Science*, 1987, **235**, 1517-1520.
35. K. Svoboda and S. M. Block, *Annu. Rev. Biophys. Biomol. Struct.*, 1994, **23**, 247-85.
36. E. Fällman, S. Schedin, J. Jass, M. Andersson, B. E. Uhlin and O. Axner*,* *Biosens. Bioel.*, 2004, **19**, 1429-1437.
37. E.Schäffer, S. F. Nørrelykke and J. Howard, *Langmuir*, 2007, **23**, 3654–3665.
38. D. Mizuno, R. Bacabac, C. Tardin, D. Head and C. F. Schmidt, *PRL*, 2009, **102**, 168102.
39. M. Tassieri, G. M. Gibson, R. M. L. Evans, A. M. Yao, R. Warren, M. J. Padgett and J. M. Cooper, *Phys. Rev. E*, 2010, **87**, 026308.
40. M. Tassieri, R. M. L. Evans, R. Warren, N. J. Bailey and J. M. Cooper, *New Journal of Physics*, 2012, **14**, 115032.
41. M. Kobayashi, M. Skarba, P. Galleto, D. Cakara and M. Borkovec, *Journal of Colloid and Interface Science*, 2005, **292**, 139-147.
42. S. H. Behrens and D. G. Grier, *J. Chem. Phys.* 2001, **115**, 6716.
43. M. J. Lang, C. L. Asbury, J. W. Shaevitz and S. M. Block, *Biophys. J.*, 2002, **83**, 491-501.
44. K. C. Vermeulen, G. J. L. Wuite, G. J. M. Stienen and C. F. Schmidt, *Appl. Optics*, 2006, **45**, 1812-1819.
45. N. Eom, V. Stevens, A. B. Wedding, R. Sedev and J. N. Connor, *Advanced Powder Technology*, 2014, **25**, 1249-1253.
46. K. Berg-Sørensen and H. Flybjerg, *Rev. Sci. Instrum.*, 2004, **75**, 594-612.
47. A. Sheikhi and R. Hill, *Soft Matter*, 2016, 12, 6575-6587.
48. H. Bruus, Theoretical Microfluidics, 1^{st} Ed., Oxford University Press, 2008.
49. P. P. Lele, J. W. Swan, J. F. Brady, N. J. Wagner and E. M. Furst, *Soft Matter*, 2011, **7,** 6844.

50. J. W. Swan and J. F. Brady, *Phys. Fluids*, 2007, **19** 113306.
51. M. Tassieri, F. Del Giudice, E. K. Robertson, N. Jain, B. Fries, R. Wilson, A. Glidle, F. Greco, P. A. Netti, P. L. Maffettone, T. Bicanica and J. M. Cooper, *Scientific Reports*, 2015, 5:8831.
52. M. Tanyeri, M. Ranka, N. Sittipolkul and C. M. Schroeder, *Lab Chip*, 2011, **11**, 1786.
53. X. Lu, C. Liu, G. Hu and X. Xuan, *Journal of Colloid and Interface Science*, 2015, **500**, 182-201

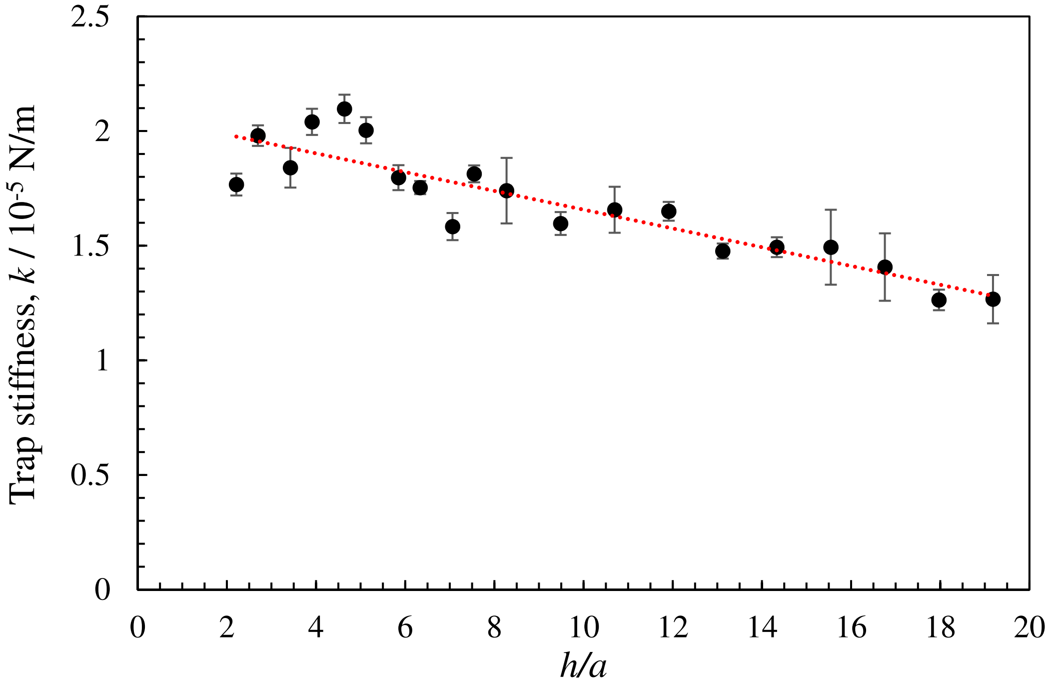

Figure 1. Trap stiffness, k of the optical trap as a function of distance from the wall h/a.

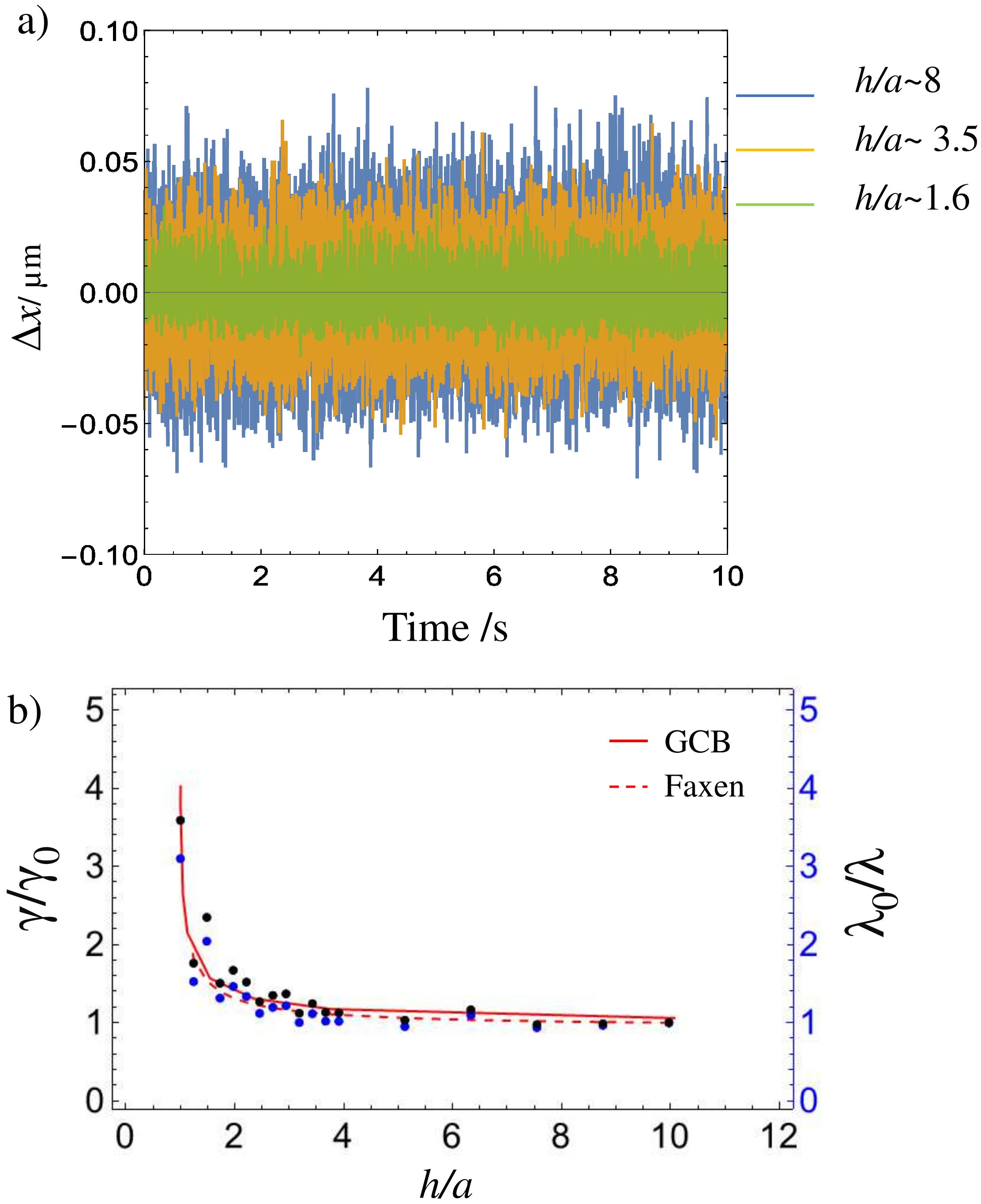

Figure 2. a) Time series of lateral position of an optically trapped particle at different height from the wall without shear flow. b) Height dependence of the normalized drag coefficient γ (black) and fit parameter λ of the normalized position autocorrelation function (blue). The dashed line indicates the fitting line from the Faxen's Law while the solid line is the exact solution of friction factor for translation by Goldman *et al*.[17]

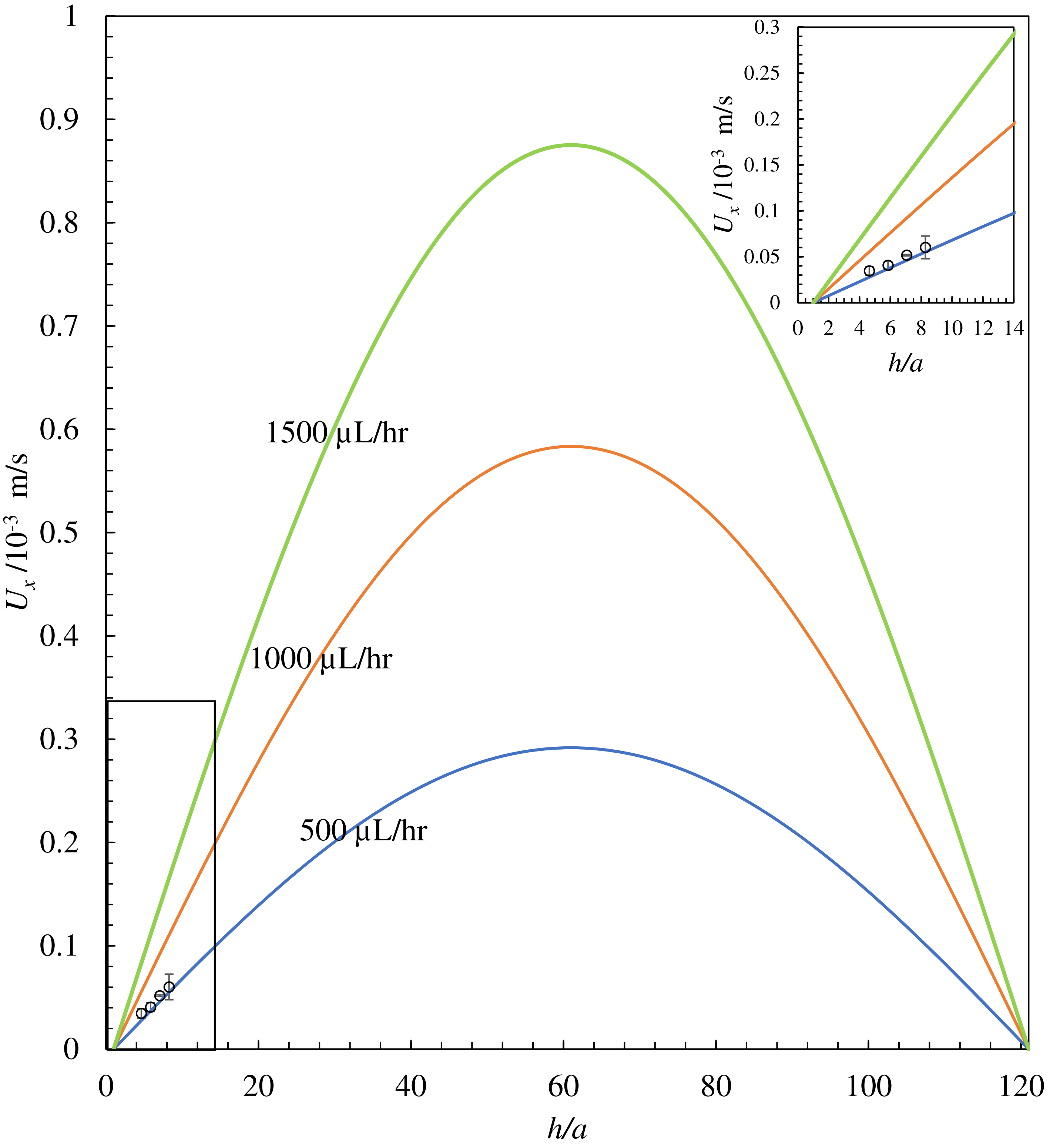

Figure 3. Theoretical fluid velocity profiles across the microchannel for different volume flow rates Q. Open symbols are the experimental local fluid velocity measured at volumetric flow rate 500 µL/hr. (Inset) Experimental region of interest.

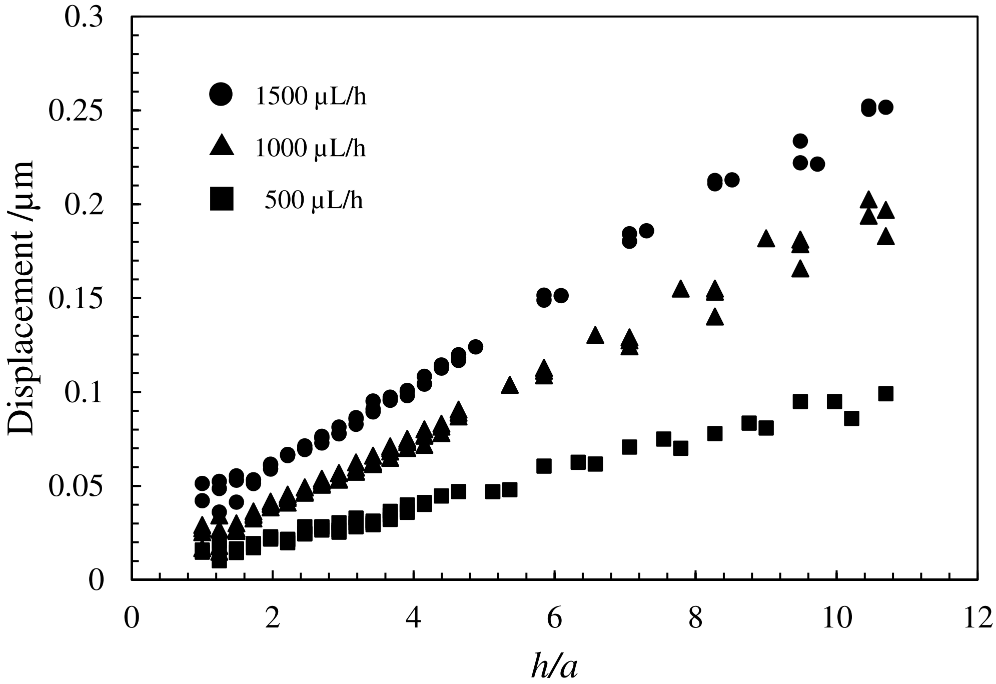

Figure 4. Displacement of the trapped particle from the equilibrium position with shear flow as a function of *h/a* at various volume flow rates *Q*.

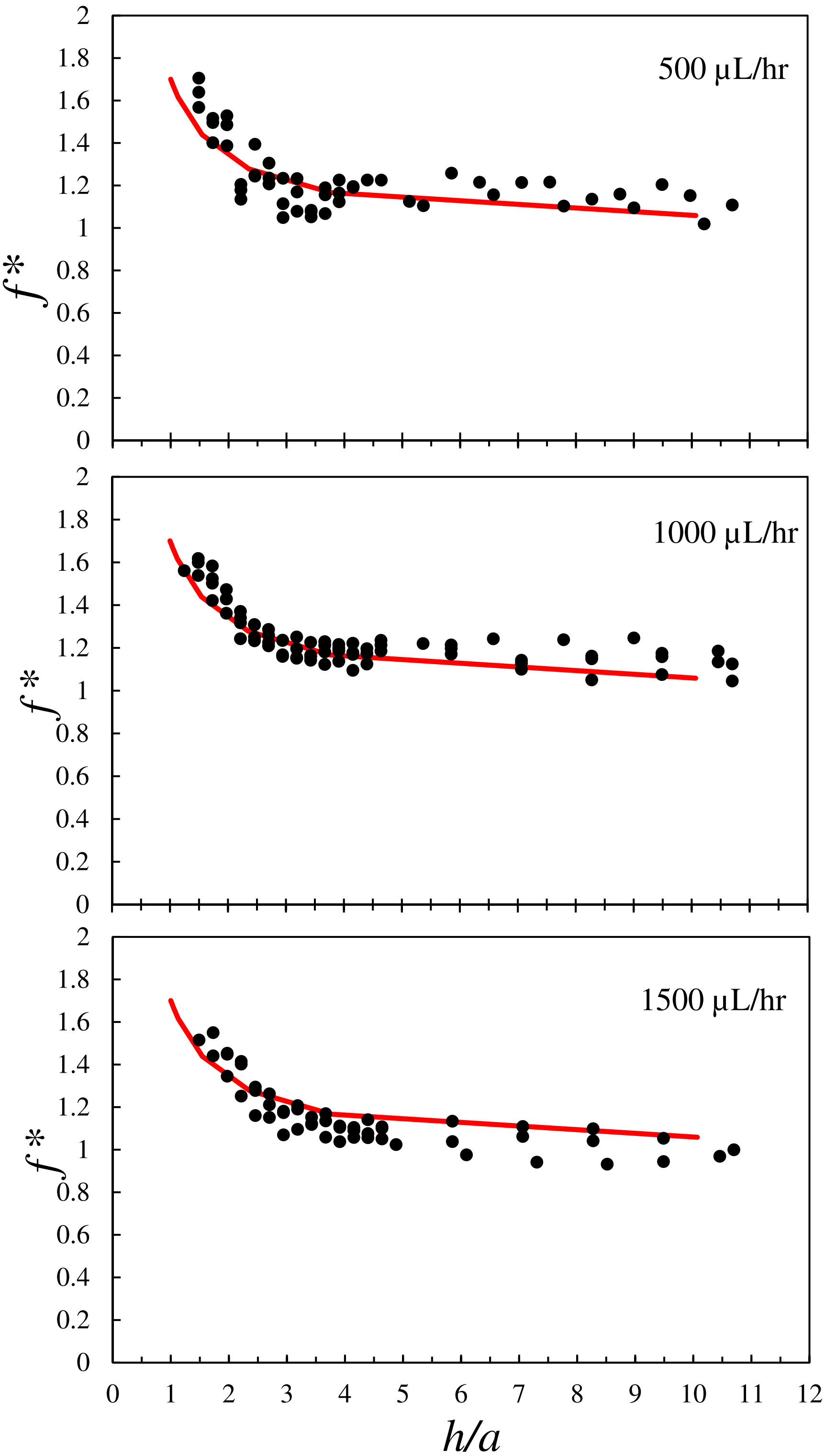

Figure 5. Experimentally calculated drag correction factor at different *h/a*. The solid red line is obtained from the exact solution of the theoretical model by Goldman *et al.*[18].